Oncogenic mutations Q61L and Q61H confer active form-like structural features to the inactive state (state 1) conformation of H-Ras protein

Matsumoto, Shigeyuki ; Taniguchi-Tamura, Haruka ; Araki, Mitsugu ; Kawamura, Takashi ; Miyamoto, Ryo ; Tsuda, Chiemi ; Shima, Fumi ;…

(Citation)
Biochemical and Biophysical Research Communications,565:85-90

(Issue Date)
2021-06-05

(Resource Type)
journal article

(Version)
Accepted Manuscript

Title: Oncogenic mutations Q61L and Q61H confer active form-like structural features to the inactive state (state 1) conformation of H-Ras protein

Authors:

Shigeyuki Matsumoto[1,a], Haruka Taniguchi-Tamura[2,a,b], Mitsugu Araki[1], Takashi Kawamura[3], Ryo Miyamoto[2], Chiemi Tsuda[2], Fumi Shima[4], Takashi Kumasaka[3], Yasushi Okuno[1,5,*] and Tohru Kataoka[2,c,*]

[1]Department of Biomedical Data Intelligence, Graduate School of Medicine, Kyoto University, 53 Shogoin-Kawaharacho, Sakyo-ku, Kyoto, 606-8507, Japan

[2]Division of Molecular Biology, Department of Biochemistry and Molecular Biology, Kobe University Graduate School of Medicine, 7-5-1 Kusunoki-cho, Chuo-ku, Kobe, 650-0017, Japan

[3]Japan Synchrotron Radiation Research Institute (JASRI), 1-1-1 Kouto, Sayo-cho, Sayo-gun, Hyogo, 679-5198, Japan

[4]Department of Drug Discovery Science, Graduate School of Science, Technology and Innovation, Kobe University, 7-5-1 Kusunoki-cho, Chuo-ku, Kobe, 650-0017, Japan

[5]RIKEN Center for Computational Science, 7-1-26 Minatojima-minami-machi, Chuo-ku, Kobe, 650-0047, Japan

[a]These authors contributed equally to this work.

[b]Present address: Carna Biosciences, Inc., BMA 3F 1-5-6 Minatojima-Minami-machi, Chuo-ku, Kobe, Hyogo, 650-0047, Japan.

[c]Present address: Kobe University Incubation Center Rm. 404, 1-5-6 Minatojima-Minami-machi, Chuo-ku, Kobe, 650-0047, Japan.

* Correspondence should be addressed to Tohru Kataoka (kataoka@people.kobe-u.ac.jp) and Yasushi Okuno (okuno.yasushi.4c@kyoto-u.ac.jp).

Abstract

GTP-bound forms of Ras proteins (Ras•GTP) assume two interconverting conformations, “inactive” state 1 and “active” state 2. Our previous study on the crystal structure of the state 1 conformation of H-Ras in complex with guanosine 5’-(β, γ-imido)triphosphate (GppNHp) indicated that state 1 is stabilized by intramolecular hydrogen-bonding interactions formed by Gln61. Since Ras are constitutively activated by substitution mutations of Gln61, here we determine crystal structures of the state 1 conformation of H-Ras•GppNHp carrying representative mutations Q61L and Q61H to observe the effect of the mutations. The results show that these mutations alter the mode of hydrogen-bonding interactions of the residue 61 with Switch II residues and induce conformational destabilization of the neighboring regions. In particular, Q61L mutation results in acquirement of state 2-like structural features. Moreover, the

mutations are likely to impair an intramolecular structural communication between Switch I and Switch II. Molecular dynamics simulations starting from these structures support the above observations. These findings may give a new insight into the molecular mechanism underlying the aberrant activation of the Gln61 mutants.

Keywords: Ras, oncogenic mutant, state transition, X-ray crystallography, molecular dynamics simulation

Introduction

The small GTPases H-Ras, K-Ras and N-Ras, collectively called Ras, are the products of the *ras* proto-oncogenes and function as on-off binary switches in diverse signaling pathways controlling cell proliferation and survival by cycling between GTP-bound active and GDP-bound inactive forms [1]. Substitution mutations predominantly involving Gly12, Gly13 and Gln61 of Ras are found in about 20% of human cancers and known to cause constitutive activation of the signaling activity mainly through impairment of their intrinsic GTPase activity [1]. Ras•GTP interact with and activate downstream effectors, such as Raf kinases and phosphoinositide 3-kinases, through two flexible regions, Switch I (residues 32–38) and Switch II (residues 60–75) [1,2]. Ras in complex with GTP or its non-hydrolyzable analogue GppNHp exhibit dynamic equilibrium between at least two interconverting conformations, termed state 1 and state 2, which were characterized by ^{31}P-NMR studies showing that either the γ- or α-phosphate group of GTP/GppNHp exhibited two resonance peaks with different chemical shift values [3,4]. Because association with c-Raf-1 induced a shift of the equilibrium toward state 2, state 1 and state 2 are regarded as “inactive” and “active” conformations, respectively. Although the crystal structure of state 2 was solved with H-Ras alone or in complex with the effectors, that of state 1 remained unsolved until we have recently succeeded in its determination for wild-type H-Ras (H-RasWT) [5] by using the humid air and glue-coating (HAG) mounting method, in which the diffraction data were acquired by regulating the surrounding humidity of crystals [6]. State 1 assumes an open structure distinguishable from state 2 by the loss of the direct and Mg^{2+}-coordinated indirect hydrogen-bonding interactions of Thr35, located in Switch I, with the γ-phosphate of GppNHp, which causes marked deviation of Switch I away from the guanine nucleotide and conformational instability of the Switch I loop (Fig. S1A). Switch II is stabilized by multiple hydrogen-bonding interactions of its Gln61 with Glu63, Tyr96 and Gln99 (Fig. S1B). Moreover, Switch II structurally communicates with Switch I through hydrogen-bonding interaction formed between Tyr71 in Switch II and Asp38 in Switch I, which plays a crucial role in effector recognition by state 2 (Fig. S1C). Intriguingly, Gln61 is one of the three mutational hotspots of Ras; mutations of Gln61 occupy about 36%, 1.3% and 60% of all the activating mutations of H-Ras, K-Ras and

N-Ras, respectively, among which Q61L and Q61H mutations occupy major populations for H-Ras and K-Ras [7]. This leads us to examine the effects of the Gln61 mutations on the tertiary structure of state 1.

In this study, we solved the state 1 crystal structures of H-RasQ61L•GppNHp and H-RasQ61H•GppNHp (H-RasQ61L$^{state\ 1}$ and H-RasQ61H$^{state\ 1}$, respectively) by using the HAG method. Comparison of their structures with that of the state 1 crystal structure of H-RasWT•GppNHp (H-RasWT$^{state\ 1}$) reveals that the mutations alter intramolecular interactions of the residue 61 with Switch II residues and perturb the neighboring region conformation. Moreover, the structural communication between Switch II and Switch I mediated by a hydrogen bond between Tyr71 and Asp38 in H-RasWT$^{state\ 1}$ is likely to be impaired in H-RasQ61L$^{state\ 1}$ and H-RasQ61H$^{state\ 1}$. These findings are well supported by MD simulations on the basis of the present crystal structures. These results may provide a new understanding of the molecular mechanism for the aberrant activation of the Gln61 mutants.

Materials and Methods

Protein preparation and purification

The catalytic domain (residues 1-166) of human H-Ras carrying Q61L or Q61H mutation was expressed as an N-terminal fusion with glutathione *S*-transferase in *Escherichia coli* BL21 (DE3) using pGEX-6P-1 vector (GE Healthcare), immobilized on glutathione-Sepharose 4B resin (GE Healthcare) and eluted by on-column cleavage with Turbo3C protease (Accelagen, California, USA) as described before [5]. It was further purified on HiTrap Q HP column (GE Healthcare), loaded with GppNHp and used for crystallization.

Crystallization and data collection

The crystals of the state 2 conformations of H-RasQ61L•GppNHp and H-RasQ61H•GppNHp were formed by using the hanging-drop vapor diffusion method at 293 K as described [5]. Subsequently, the HAG method was applied to the crystals to induce transition of state 2 to state 1 in crystals. The state 1 crystals were flash-cooled under nitrogen stream, and diffraction data were collected on beamline BL38B1 at SPring-8 and processed with the HKL2000 program [8] and the CCP4 program suite [9]. Structural refinement was proceeded by using the PHENIX program [10] and COOT [11]. Crystallographic and X-ray data statistics are summarized in Table 1. Atomic coordinates and structure factors for H-RasQ61L$^{state\ 1}$ and H-RasQ61H$^{state\ 1}$ were deposited in the Protein Data Bank (PDB; http://www.rcsb.org) under accession codes 7DPJ and 7DPH, respectively.

Molecular dynamics simulations

The initial coordinates of H-RasWT$^{state\ 1}$ were derived from PDB (entry: 5B30). The disordered region of Switch II in H-RasQ61H$^{state\ 1}$ was modeled from the atomic models of H-

RasQ61L$^{state\ 1}$ or H-RasWT$^{state\ 1}$ by using the Molecular Operating Environment (MOE, Chemical Computing Group, Montreal, Canada), version 2016.08. The data obtained from the model with Q61L-derived Switch II were mainly used unless otherwise stated. Addition of the hydrogen atoms and generation of the topology files were carried out by using a pdb2gmx module in the GROMACS package 2016 [12]. The electrostatic potential for GppNHp was calculated using the General Atomic and Molecular Electronic Structure System (GAMESS) program [13] at the RHF/6–31G* level, and thereby the atomic partial charges were assigned by the restrained electrostatic potential (RESP) approach [14]. Other parameters for GppNHp were determined by the general Amber force field (GAFF) using the antechamber module of AMBER Tools [15,16]. Approximately 6,300 water molecules were placed around the complex model with an encompassing distance of 10 Å to form a $65.9 \times 62.1 \times 53.8$ Å^3 periodic boxes. Flat-bottom potentials with force constants of 10 kJ/mol/Å^2 were applied to restrain the distances between Mg^{2+} ions and their coordinating atoms during the simulation. Other simulation parameters were identical with those used before [17] and two-hundred nanosecond production runs with five different initial velocities were carried out for each protein system by using the GROMACS 2016.5 on High Performance Computing Infrastructure equipped with NVIDIA GeForce GTX 1080Ti GPGPUs. The MD trajectories were analyzed by the GROMACS package, PyMOL (DeLano Scientific, LLC) and High Throughput Molecular Dynamics (HTMD) environment 1.14.0. [18].

Results

Overall structures of H-RasQ61L$^{state\ 1}$ and H-RasQ61H$^{state\ 1}$

We solved the crystal structures of H-RasQ61L$^{state\ 1}$ and H-RasQ61H$^{state\ 1}$ at the resolution of 1.97 Å and 1.54 Å, respectively (Table S1). They both showed open conformations which lost the hydrogen-bonding interactions of Thr35 with the γ-phosphate of GppNHp resulting in marked deviation of Switch I away from the guanine nucleotide, the hallmark of the state 1 conformation (Fig. S2A). The backbone structures were very similar to that of H-RasWT$^{state\ 1}$ (PDB entry 5B30) except for Switch II (Fig. 1A), whose electron densities became quite poor compared to the other part suggesting high flexibility. Switch II of H-RasQ61L$^{state\ 1}$ was positioned closer to GppNHp in comparison with that of H-RasWT$^{state\ 1}$ (Fig. 1A and Fig. S2 B and C). On the other hand, a majority of Switch II (residues 62–69) of H-RasQ61H$^{state\ 1}$ was grossly disordered, providing less structural information (Fig. 1A and Fig. S2D).

Mutation-induced structural perturbations in Switch II and its neighboring regions

In the H-RasWT$^{state\ 1}$ structure, Switch II is stabilized by three hydrogen bonds formed by Gln61: one between the side chain nitrogen atom of Gln61 and the backbone oxygen atom of Glu63, one between the backbone nitrogen atom of Gln61 and the side chain oxygen atom of

Tyr96 and the other between the side chain oxygen atom of Gln61 and the side chain nitrogen atom of Gln99 (Fig. S1B). In the H-RasQ61L$^{state\ 1}$ structure, Leu61 formed not only a hydrogen bond with Tyr96 but also a hydrophobic contact with the aromatic ring of Tyr96, thereby inducing reorientation of the side chain conformation of Leu61 while it failed to form hydrogen bonds with Glu63 and Gln99 (Fig. 1B). The reorientation of the side chain of Leu61 was accompanied by large changes in the backbone dihedral angles (φ, ψ) from (-137.8, 115.1) to (-60.9, -25.9), orienting the backbone oxygen atom toward a position partly overlapping with that occupied by the backbone nitrogen atom of Glu63 in H-RasWT$^{state\ 1}$ (Fig. 2A). These local structural changes were expected to induce a positional change of Glu63 toward GppNHp, impairing intramolecular interactions formed by this residue. These conformational changes may account for the global positional movement of Switch II toward GppNHp observed for H-RasQ61L$^{state\ 1}$. In the H-RasQ61H$^{state\ 1}$ structure, the electron density of the side chain of His61 was not observed, suggesting that the residue adopted variable conformations (Fig. 1C).

In the H-RasWT$^{state\ 1}$ structure, the side chain of Tyr71 is stabilized by a hydrophobic contact with Leu56 and a hydrogen bonding interaction with Asp38 in Switch I (Fig. S1C). In the H-RasQ61L$^{state\ 1}$ structure, these interactions appeared to be disrupted because there were no interpretable electron densities for the side chain of Tyr71 and Leu56 (Fig. S3A). Similarly, the side chain of Tyr71 in the H-RasQ61H$^{state\ 1}$ structure appeared to adopt variable conformations because there was no interpretable electron density for the side chain of Tyr71 (Fig. S3B). These structural changes found in the two mutants are likely to impair the Asp38-mediated conformational communication between Switch I and Switch II. Nevertheless, not only the backbone structures of Switch I but also the side chain structure of Asp38 in the two mutants looked nearly identical to that of H-RasWT$^{state\ 1}$ (Fig. 2B), prompting us to investigate the in-solution conformations using molecular dynamics (MD) simulations.

Impact of the residue 61 mutations on the dynamic behaviors of Switch I and Switch II

To investigate in-solution behaviors of H-RasQ61L$^{state\ 1}$ and H-RasQ61H$^{state\ 1}$, we performed 200 nsec-length MD simulations with five independent initial velocities using the solved state 1 crystal structures as initial models. The disordered region in H-RasQ61H$^{state\ 1}$ was modeled on the basis of the atomic models of H-RasWT$^{state\ 1}$ or H-RasQ61L$^{state\ 1}$. The MD-derived root-mean square fluctuations (RMSF) representing the atomic fluctuations of the Cα atoms around the mean structure showed that a part of Switch II (Glu63-Met67) of H-RasQ61H$^{state\ 1}$ was found to be more flexible for the both models than those of H-RasWT$^{state\ 1}$ or H-RasQ61L$^{state\ 1}$ (Fig. 3 and Fig. S4). This in-solution behavior specific to H-RasQ61H agreed well with the crystallographic observation that the electron density at the corresponding region was absent in H-RasQ61H$^{state\ 1}$. In addition, the flexibility of the C terminal regions of Switch I (Glu37 and Asp38) was significantly elevated although they are spatially distant from His61 (Fig. 3 and Fig. S4). Similar

conformational destabilization in the Switch I region was observed for H-RasQ61L$^{state\ 1}$, albeit less obvious (Fig. 3).

The principal component analysis (PCA) of the Switch II conformations emerging in the MD simulations showed that the conformational states of H-RasQ61L$^{state\ 1}$ were significantly different from those of H-RasWT$^{state\ 1}$ (Fig. 4A). The pairwise comparison of the MD-derived mean structures for H-RasWT^{state1} and H-RasQ61L$^{state\ 1}$ with several state 2 crystal structures showed that the Switch II configuration of H-RasQ61L$^{state\ 1}$ was similar to those of the H-RasWT•GppNHp state 2 (H-RasWT$^{state\ 2}$) structure alone or the oncogenic mutants in complex with the effectors, indicating that Q61L mutation induced conformational transition of Switch II toward state 2 (Fig. 4B). This MD-based observation agreed well with the present crystallographic study on H-RasQ61L$^{state\ 1}$, in which Switch II came closer to GppNHp. In H-RasQ61H$^{state\ 1}$, although the simulated conformations were affected by the initial models to some extent, it looked that they preferably sampled the conformations observed in H-RasQ61L$^{state\ 1}$ rather than H-RasWT^{state1} (Fig. 4A and Fig. S5).

The Switch I conformations of H-RasQ61L$^{state\ 1}$ and H-RasQ61H$^{state\ 1}$ in the crystal structures looked not significantly different from that of H-RasWT$^{state\ 1}$ (Fig. 1A) even though the mutation-induced conformational changes of their Switch II are likely to impair the structural communication between Switch II and Switch I mediated by a hydrogen bond between Tyr71 and Asp38 in H-RasWT$^{state\ 1}$ (Fig. 2B and Fig. S3). However, calculation of the root-mean square deviations (RMSD) of MD-derived Asp38 from the initial structures showed that its deviated conformations were observed in H-RasQ61L$^{state\ 1}$ and H-RasQ61H$^{state\ 1}$ during the simulations whereas those in H-RasWT$^{state\ 1}$ were relatively stable during the simulations (Fig. 4C).

Discussion

In the present study, we show that an oncogenic mutant Q61L confers state 2-like configurations upon Switch II of the inactive conformational state, state 1, of H-Ras, which plays a crucial role in effector recognition by state 2. Also, another mutation Q61H is likely to confer increased structural flexibility to Switch II and result in acquisition of structural features similar to H-RasQ61L$^{state\ 1}$ although the structural information was rather limited. Moreover, the two mutations result in disruption of the structural communication between Switch II and Switch I and conformational displacement of Asp38, which also plays a crucial role in effector recognition by state 2 [19]. The displacement of Asp38 may exert a favorable effect for capturing the effector molecules by freeing its side chain from restriction by way of a hydrogen-bonding interaction with Tyr71. Recent MD and NMR studies on the structure of post-translationally modified K-RasWT•GppNHp (PDB entry 2MSD) anchored on the lipid bilayer membranes indicated that the orientation of the catalytic domain on the cellular membrane adopts at least two orientations: an

occluded orientation in which the switch regions are masked by the membrane surface and an exposed orientation in which they are available for interaction with the effectors [20,21] (Fig. S6). Thus, the dynamic changes in Switch II of H-RasQ61H$^{state\ 1}$ may affect the orientations of Ras on the cellular membranes; the elevation of the flexibility is likely to be entropically unfavorable for adoption of the occluded orientation, thereby shifting the equilibrium toward the exposed orientation. Taken together, the conformational changes occurred in H-RasQ61L and H-RasQ61H are likely to enhance the signaling activity of Ras by facilitating the transition of inactive states toward active states.

A wide variety of mutations of Ras were found in human cancer and the signaling and oncogenic activities of the mutants were reported to be variable, suggesting that some differences might exist in the molecular mechanisms for their activation. In general, the activation mechanism of the Gly12 and Gln61 mutants is accounted for by impairment of their intrinsic GTPase activity, which is known to depend on the location and orientation of the side chain of Gln61 and of two water molecules (Wat-175 and Wat-189) activated by the side chain of Gln-61 to exert a nucleophilic attack on the γ-phosphate of GTP [22]. The bulky Val12 side chain of the G12V mutant is thought to lower the GTPase activity through a steric interference over this catalytic process. The present study suggests that another mechanism might play a role in activation of the Gln61 mutants, whose significance must be further addressed by future studies.

Author contributions

S.M., H.T., and T.KAT. designed the study. H.T., R.M., and C.T. expressed, purified, and crystallized H-RasQ61L•GppNHp and H-RasQ61H•GppNHp. H.T., T.KAW., and T.KU. collected diffraction data with HAG methods and refined the structures. S.M., H.T., and F.S. analyzed the crystal structure. S.M., M.A., and Y.O. performed the molecular dynamics simulation and analyzed the trajectory data. S.M. and H.T. wrote the manuscript. All authors discussed the research, edited the manuscript and approved its final version.

Data availability

Coordinates of H-RasQ61L$^{state\ 1}$ and H-RasQ61H$^{state\ 1}$ have been deposited in the Protein Data Bank, under the accession number 7DPJ and 7DPH, respectively.

Acknowledgement

We thank Dr. Seiki Baba for his help with X-ray data collection using the HAG method. The synchrotron radiation experiments were performed at the BL38B1 of SPring-8 with the approval of the Japan Synchrotron Radiation Research Institute (JASRI) (Proposal No. 2016A2515, 2017A2583 and 2017B2583). This work was supported by JSPS KAKENHI Grant Number

JP17K15106 to SM.

Declaration of Interests

The authors declare no competing interests.

Figure legends

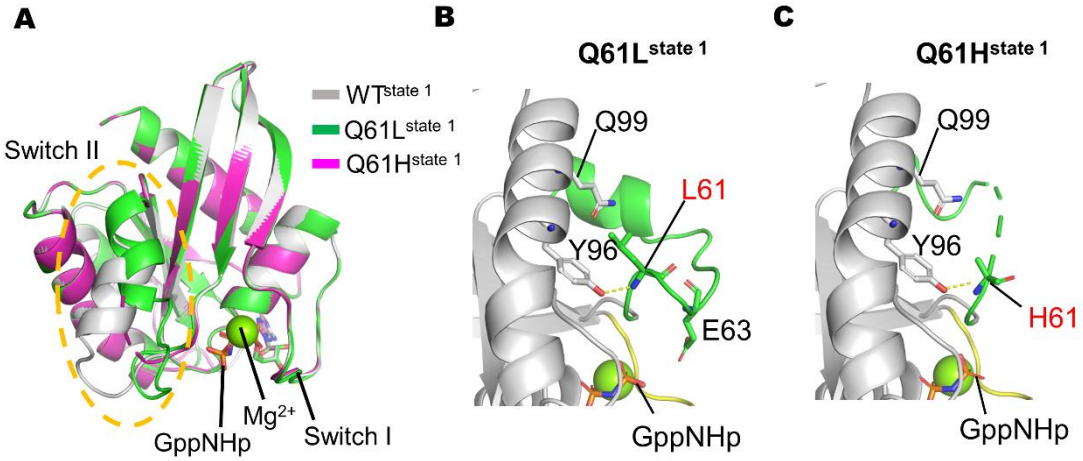

Fig. 1. Mutation-induced structural perturbation in Switch II. (A) Superimposition of crystal structures of H-RasWT$^{state\ 1}$ (gray), H-RasQ61L$^{state\ 1}$ (green), and H-RasQ61H$^{state\ 1}$ (magenta). GppNHp and a magnesium ion are represented by the stick and sphere models, respectively. Switch II region is indicated by an orange dashed circle. Enlarged views of the region proximal to the residue 61 for H-RasQ61L$^{state\ 1}$ (B), and H-RasQ61H$^{state\ 1}$ (C). Hydrogen bonds formed by Leu/His61 are indicated by yellow dashed lines. Switch II regions are colored green. Residues discussed in the main text are represented by the stick model. Disordered backbone region is indicated by a dashed line.

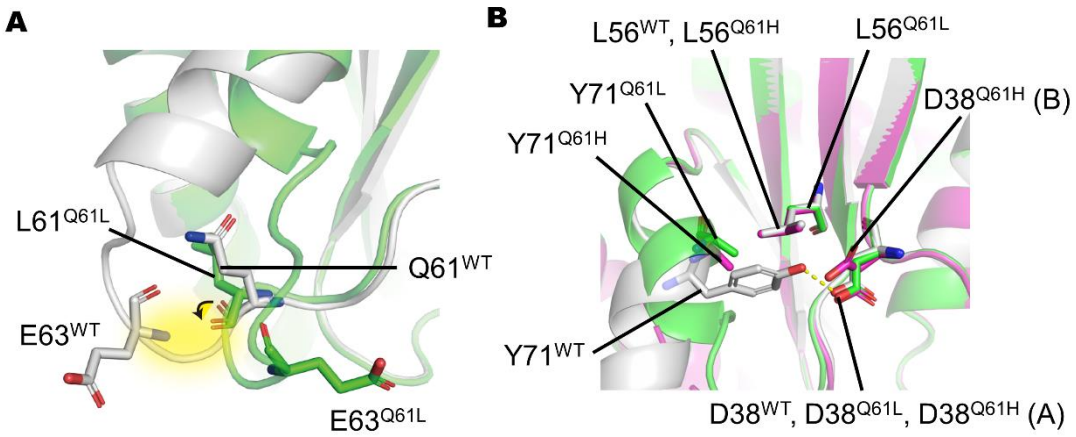

Fig. 2. Comparison of the key hydrogen bond interactions of the Q61L/Q61H mutants with those of wild-type. H-RasWT$^{state\ 1}$, H-RasQ61L$^{state\ 1}$, and H-RasQ61H$^{state\ 1}$ are colored gray, green and magenta, respectively. (A) Mutation-induced steric hindrance of Leu61 of H-RasQ61L$^{state\ 1}$ with Glu63 of H-RasWT$^{state\ 1}$. A region of Leu61 possibly overlapped with Glu63 is highlighted by yellow. The reorientation of the backbone oxygen atom of Leu61 is indicated by a black arrow. (B) Disruption of structural communication between Switch I and Switch II. A hydrogen bond formed between Tyr71 and Asp38 of H-RasWT$^{state\ 1}$ is indicated by a yellow dashed line. The side chains of Leu56 in H-RasQ61L$^{state\ 1}$ and Tyr71 in both H-RasQ61L$^{state\ 1}$ and H-RasQ61H$^{state\ 1}$ are disordered. The side chain of Asp38 in H-RasQ61H$^{state\ 1}$ adopts an alternative conformation exhibiting two distinct orientations, one of which (alternative conformation A) is nearly identical to that of H-RasWT$^{state\ 1}$ and labeled as (A). The other one is oriented toward the bulk solvent and labeled as (B).

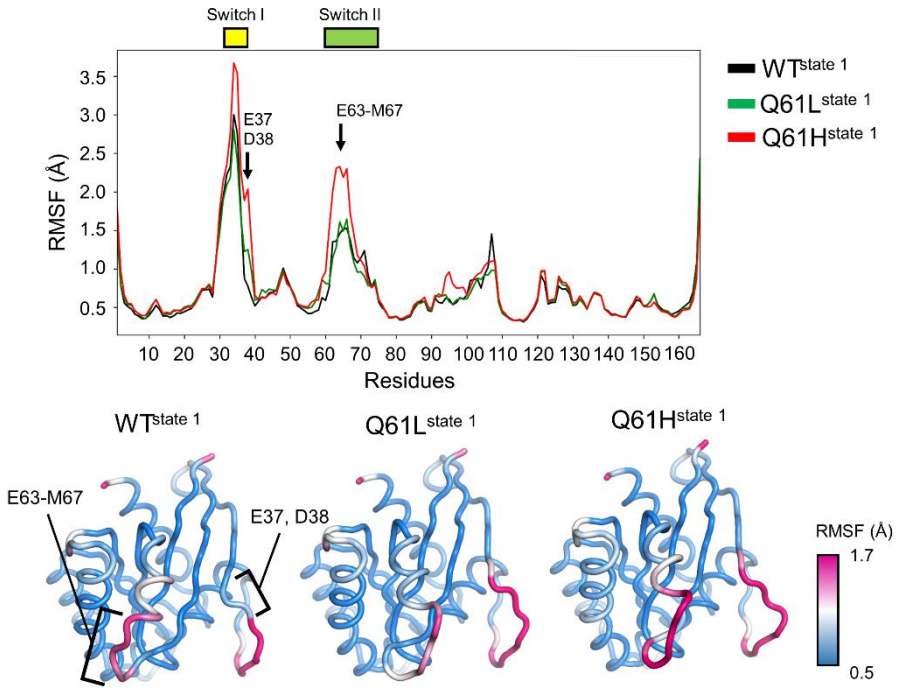

Fig. 3. Residual fluctuations of H-RasWT$^{state\ 1}$, H-RasQ61L$^{state\ 1}$ and H-RasQ61H$^{state\ 1}$ in solution. The RMSF values are calculated for the Cα atoms. The values for H-RasWT$^{state\ 1}$ and H-RasQ61L$^{state\ 1}$ are indicated by black and green lines, respectively (upper panel). For H-RasQ61H$^{state\ 1}$, the value obtained for the model with the Q61L mutant-derived Switch II is indicated by a red line. The RMSF values are mapped onto the MD-derived mean structures by gradual color changes (lower panels).

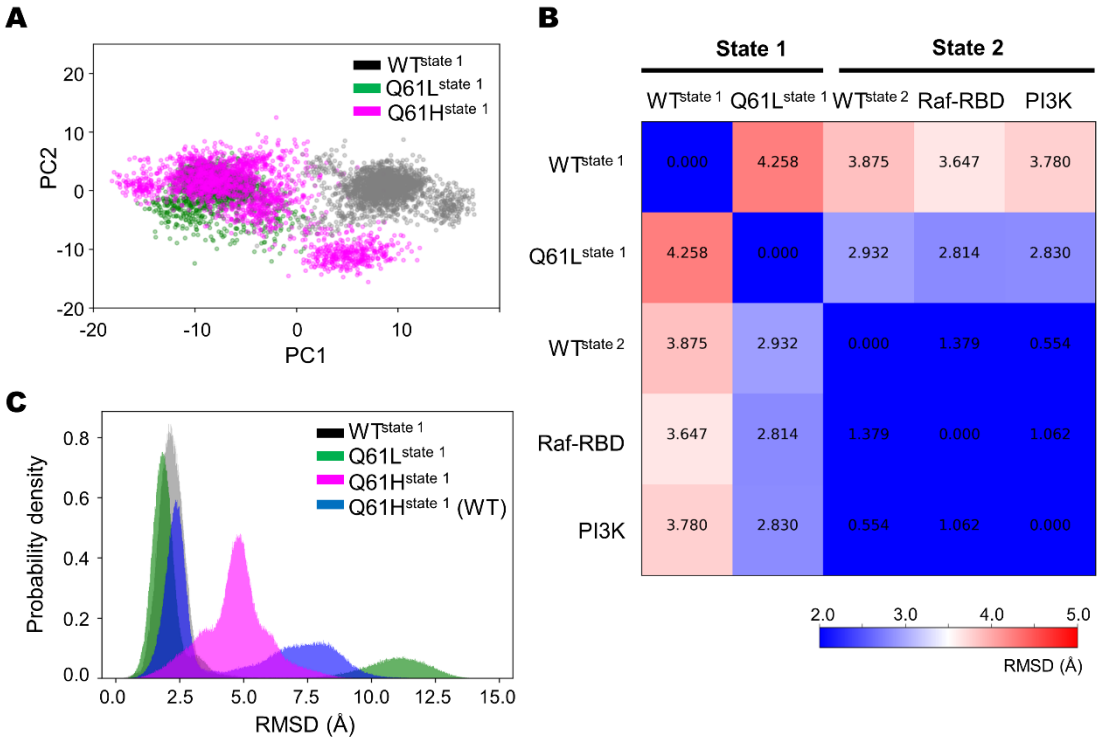

Fig. 4. Impact of Q61L/Q61H mutations on the dynamic behavior of the switch regions. (A) Conformational distribution of Switch II in H-RasWT$^{state\ 1}$ (gray), H-RasQ61L$^{state\ 1}$ (green) and H-RasQ61H$^{state\ 1}$ with the Q61L mutant-derived Switch II on the PCA planes. PCA is carried out using the Switch II conformations emerging during the MD simulations. (B) Structural comparison of the MD-derived mean structure of Switch II in H-RasWT$^{state\ 1}$ and H-RasQ61L$^{state\ 1}$ with several state 2 structures. The crystal structures of H-RasWT$^{state\ 2}$ (3K8Y), H-RasQ61L$^{state\ 2}$ in complex with the Ras-binding domain of c-Raf-1 (4G3X), and H-RasG12V$^{state\ 2}$ in complex with phosphoinositide 3-kinase (1HE8) are selected for the structural comparison. The RMSD values of Switch II are calculated for all pairs and indicated along with the values, i.e., blue color denotes the similar structure. (C) Distribution of RMSD values of MD-derived Asp38 conformations against the initial structures. The distributions of H-RasWT$^{state\ 1}$, H-RasQ61L$^{state\ 1}$ and H-RasQ61H$^{state\ 1}$ are colored gray, green and magenta, respectively. The distribution of H-RasQ61H$^{state\ 1}$ whose initial model is constructed on the basis of the atomic structure of H-RasWT$^{state\ 1}$ is colored blue. Larger values indicate occurrence of more significant conformational displacements from the initial crystal structure. The alternative conformation A defined in Fig. 2B is used as the initial structure in H-RasQ61H$^{state\ 1}$.

References

[1] A.E. Karnoub, R.A. Weinberg, Ras oncogenes: split personalities, Nature reviews. Molecular cell biology 9 (2008) 517-531. 10.1038/nrm2438.

[2] A. Wittinghofer, H. Waldmann, Ras—A Molecular Switch Involved in Tumor Formation, Angew Chem Int Ed Engl. 39 (2000) 4192-4214. 10.1002/1521-3773(20001201)39:23<4192::AID-ANIE4192>3.0.CO;2-Y.

[3] M. Geyer, T. Schweins, C. Herrmann, T. Prisner, A. Wittinghofer, H.R. Kalbitzer, Conformational transitions in p21ras and in its complexes with the effector protein Raf-RBD and the GTPase activating protein GAP, Biochemistry 35 (1996) 10308-10320. 10.1021/bi952858k.

[4] M. Spoerner, C. Hozsa, J.A. Poetzl, K. Reiss, P. Ganser, M. Geyer, H.R. Kalbitzer, Conformational states of human rat sarcoma (Ras) protein complexed with its natural ligand GTP and their role for effector interaction and GTP hydrolysis, The Journal of biological chemistry 285 (2010) 39768-39778. 10.1074/jbc.M110.145235.

[5] S. Matsumoto, N. Miyano, S. Baba, J. Liao, T. Kawamura, C. Tsuda, A. Takeda, M. Yamamoto, T. Kumasaka, T. Kataoka, F. Shima, Molecular Mechanism for Conformational Dynamics of Ras.GTP Elucidated from In-Situ Structural Transition in Crystal, Sci Rep 6 (2016) 25931. 10.1038/srep25931.

[6] S. Baba, T. Hoshino, L. Ito, T. Kumasaka, Humidity control and hydrophilic glue coating applied to mounted protein crystals improves X-ray diffraction experiments, Acta crystallographica. Section D, Biological crystallography 69 (2013) 1839-1849. 10.1107/S0907444913018027.

[7] I.A. Prior, P.D. Lewis, C. Mattos, A comprehensive survey of Ras mutations in cancer, Cancer research 72 (2012) 2457-2467. 10.1158/0008-5472.CAN-11-2612.

[8] Z. Otwinowski, W. Minor, [20] Processing of X-ray diffraction data collected in oscillation mode, in: Charles W. Carter, Jr. (Ed.) Methods in Enzymology, Academic Press1997, pp. 307-326.

[9] M.D. Winn, C.C. Ballard, K.D. Cowtan, E.J. Dodson, P. Emsley, P.R. Evans, R.M. Keegan, E.B. Krissinel, A.G.W. Leslie, A. McCoy, S.J. McNicholas, G.N. Murshudov, N.S. Pannu, E.A. Potterton, H.R. Powell, R.J. Read, A. Vagin, K.S. Wilson, Overview of theCCP4 suite and current developments, Acta Crystallographica Section D Biological Crystallography 67 (2011) 235-242. 10.1107/s0907444910045749.

[10] D. Liebschner, P.V. Afonine, M.L. Baker, G. Bunkóczi, V.B. Chen, T.I. Croll, B. Hintze, L.-W. Hung, S. Jain, A.J. McCoy, N.W. Moriarty, R.D. Oeffner, B.K. Poon, M.G. Prisant, R.J. Read, J.S. Richardson, D.C. Richardson, M.D. Sammito, O.V. Sobolev, D.H. Stockwell, T.C. Terwilliger, A.G. Urzhumtsev, L.L. Videau, C.J. Williams, P.D. Adams, Macromolecular structure determination using X-rays, neutrons and electrons: recent developments in Phenix, Acta Crystallographica Section D Structural Biology 75 (2019) 861-877. 10.1107/s2059798319011471.

[11] P. Emsley, B. Lohkamp, W.G. Scott, K. Cowtan, Features and development ofCoot, Acta Crystallographica Section D Biological Crystallography 66 (2010) 486-501.

10.1107/s0907444910007493.
[12] M.J. Abraham, T. Murtola, R. Schulz, S. Páll, J.C. Smith, B. Hess, E. Lindahl, GROMACS: High performance molecular simulations through multi-level parallelism from laptops to supercomputers, SoftwareX 1-2 (2015) 19-25. 10.1016/j.softx.2015.06.001.
[13] M.W. Schmidt, K.K. Baldridge, J.A. Boatz, S.T. Elbert, M.S. Gordon, J.H. Jensen, S. Koseki, N. Matsunaga, K.A. Nguyen, S. Su, T.L. Windus, M. Dupuis, J.A. Montgomery, General atomic and molecular electronic structure system, Journal of Computational Chemistry 14 (1993) 1347-1363. 10.1002/jcc.540141112.
[14] C.I. Bayly, P. Cieplak, W. Cornell, P.A. Kollman, A well-behaved electrostatic potential based method using charge restraints for deriving atomic charges: the RESP model, The Journal of Physical Chemistry 97 (1993) 10269-10280. 10.1021/j100142a004.
[15] A.W. Sousa da Silva, W.F. Vranken, ACPYPE - AnteChamber PYthon Parser interfacE, BMC Research Notes 5 (2012). 10.1186/1756-0500-5-367.
[16] J. Wang, R.M. Wolf, J.W. Caldwell, P.A. Kollman, D.A. Case, Development and testing of a general amber force field, Journal of Computational Chemistry 25 (2004) 1157-1174. 10.1002/jcc.20035.
[17] S. Matsumoto, M. Araki, Y. Isaka, F. Ono, K. Hirohashi, S. Ohashi, M. Muto, Y. Okuno, E487K-Induced Disorder in Functionally Relevant Dynamics of Mitochondrial Aldehyde Dehydrogenase 2, Biophys J 119 (2020) 628-637. 10.1016/j.bpj.2020.07.002.
[18] S. Doerr, M.J. Harvey, F. Noé, G. De Fabritiis, HTMD: High-Throughput Molecular Dynamics for Molecular Discovery, Journal of Chemical Theory and Computation 12 (2016) 1845-1852. 10.1021/acs.jctc.6b00049.
[19] S.K. Fetics, H. Guterres, B.M. Kearney, G. Buhrman, B. Ma, R. Nussinov, C. Mattos, Allosteric effects of the oncogenic RasQ61L mutant on Raf-RBD, Structure (London, England : 1993) 23 (2015) 505-516. 10.1016/j.str.2014.12.017.
[20] M.T. Mazhab-Jafari, C.B. Marshall, M.J. Smith, G.M.C. Gasmi-Seabrook, P.B. Stathopulos, F. Inagaki, L.E. Kay, B.G. Neel, M. Ikura, Oncogenic and RASopathy-associated K-RAS mutations relieve membrane-dependent occlusion of the effector-binding site, Proceedings of the National Academy of Sciences 112 (2015) 6625-6630. 10.1073/pnas.1419895112.
[21] P. Prakash, Y. Zhou, H. Liang, J.F. Hancock, A.A. Gorfe, Oncogenic K-Ras Binds to an Anionic Membrane in Two Distinct Orientations: A Molecular Dynamics Analysis, Biophysical Journal 110 (2016) 1125-1138. 10.1016/j.bpj.2016.01.019.
[22] E.F. Pai, U. Krengel, G.A. Petsko, R.S. Goody, W. Kabsch, A. Wittinghofer, Refined crystal structure of the triphosphate conformation of H-ras p21 at 1.35 A resolution: implications for the mechanism of GTP hydrolysis, The EMBO journal 9 (1990) 2351-2359.